Downloaded from https://iranpaper.ir
https://www.tarjomano.com/order
ترجمه تخصصی این مقاله

Copyright © Smart/Micro Grid Research Center, 2020

Electric Power Systems Research 174 (2019) 105863

Contents lists available at ScienceDirect

Electric Power Systems Research

journal homepage: www.elsevier.com/locate/epsr

Bulk power system frequency stability assessment in presence of microgrids

Hêmin Golpîra

Department of Electrical and Computer Engineering, University of Kurdistan, Kurdistan, Sanandaj, Iran

ARTICLE INFO

Keywords:
Frequency stability
Model validation
Distributed generation
Rotational inertia
Inverter based sources
Genset

ABSTRACT

An attempt is made in this paper to propose an analytical approach to mathematically assess the impact of MGs penetration level on power system frequency stability. Firstly, experimental-based model of constitute DGs of the University of Kurdistan-MG (UOK-MG) in islanded mode may be derived. Afterwards, realistic model of the MG in grid connected mode may be derived to realize penetrated system for future studies. Finally, some simple algebraic equations are derived to predict frequency dynamics of interest in penetrated system. The method interprets the frequency dynamic behavior of the penetrated system based on the conventional system in terms of frequency nadir, Rate of Change of Frequency (*RoCoF*), steady state deviation and a rolling window. Simulation results demonstrate high efficiency of the proposed approach for dynamical modeling and stability analysis of penetrated power systems.

1. Introduction

Modern power networks face new technical challenges arising from the increasing penetration of Distributed Generations (DGs), visualized through the Microgrid (MG) concept. While low penetration of MGs has negligible influence on host grid stability, high level of penetration may affect system reliability and create voltage and frequency issues that must be addressed [1–3]. The present paper aims to analytically deal with host grid frequency dynamics in presence of MGs.

Due to the physical characteristics of DGs, including special connection to grid via inverters, their interactions with the grid are different from those of conventional generating units. In this way, inertia constant, which buys controllers and operators time to keep the system secure, significantly reduces in penetrated grids [4,5]. Indeed, low inertia feature in systems with high MGs penetration level renders frequency dynamics faster and thus jeopardizes system stability [6,7].

General overview regarding the effects of low inertia feature on power system frequency stability has been provided in Refs. [5,7]. A trial and error-based methodology is discussed in Refs. [8,9] to determine maximum permissible penetration level of wind farms. Transit stability assessment of penetrated power system is done in Refs. [10,11]. Scenario-based approach of Ref. [12] focuses on system inertia and primary reserve values. Simplified frequency model of the system is incorporated with a simulation-based approach to study frequency behavior of a penetrated power grid in Refs. [13]. Another scenario-based approach, applied to a part of Australian grid, is discussed in Ref. [14]. Ref. [15] proposes a framework for assessing renewable integration limits concerning power system frequency performance using a time-series scenario based approach. A new automatic generation control structure, which tackles intermittency drawbacks stemming from high penetration of MGs into problem formulation, is proposed in Ref. [16]. In another attempt, a frequency-domain model to evaluate AGC performances under wind power uncertainty is presented in Ref. [17].

While previous studies deal with the effects of MGs penetration level on host grid stability, most of them have varied the penetration level on low dimension systems based on trial and error. Following trial and error approaches, Transmission System Operators (TSOs) should define a set of probable operating conditions to be assessed during Time Domain Simulation (TDS) procedure. Highly uncertain behavior of MGs besides high dimensions of real power systems cause the volume of scenarios becomes daunting, which in turn, presents a problem of finding a valid set of operating points. Therefore, the so far researches, for example [6,15], consider constant parameters, usually worst case inertia constant, for the MGs in the trial and error procedure which is an unrealistic assumption. On the other hand, the recent researches in the field mainly focus on inertia reduction rather than MG penetration level and hence the effects of MG dynamics and structure are neglected. This means that the penetrated grid in the so far researches usually visualized by reducing of generating unit inertia constants. This in turn causes the results do not have any physical meaning, thereby offering limited insight to power system engineers and power system planners concerning host grid dynamics. While developing equivalent models for MGs, able to account for stability assessment, have been recently proposed in the literature [18–22], but their efficiency has only been tested using simulation results. Thus, their applicability for real field applications remains an open issue. To overcome such crudities, a new

E-mail address: hemin.golpira@uok.ac.ir.

https://doi.org/10.1016/j.epsr.2019.105863
Received 29 July 2018; Received in revised form 25 January 2019; Accepted 29 April 2019
Available online 09 May 2019
0378-7796/ © 2019 Elsevier B.V. All rights reserved.

Downloaded from https://iranpaper.ir
https://www.tarjomano.com/order
ترجمه تخصصی این مقاله

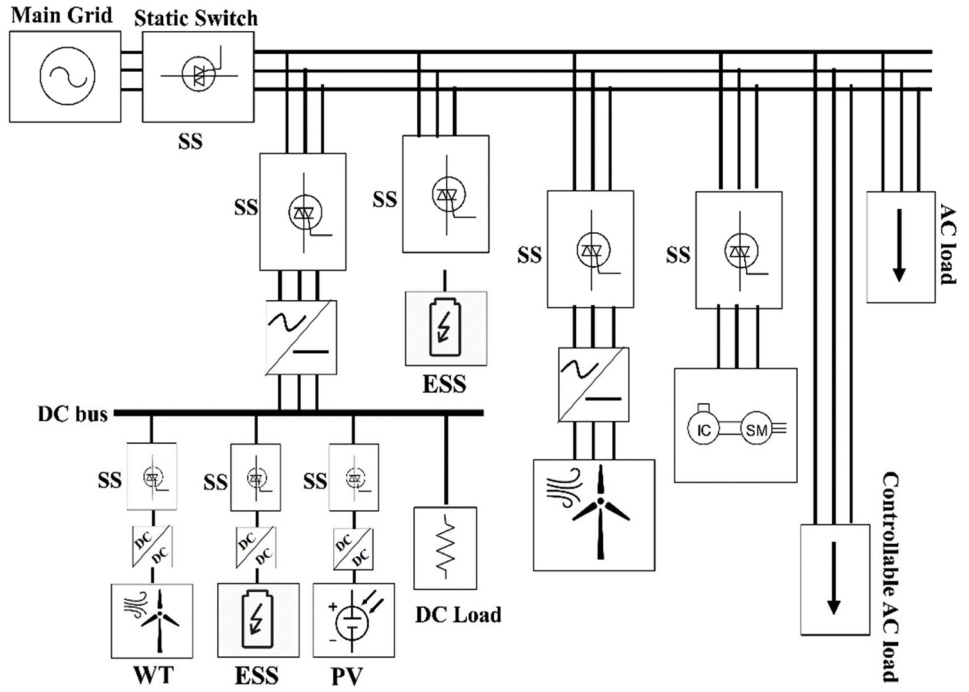

(a)

(b)

Fig. 1. UOK-MG schematic. (a) Three-phase representation, and (b) constituent components.

methodology to derive a simple physically defined equivalent model of MG from upward frequency stability point of view is proposed. Afterwards, MG penetration level may be tied to the inertia constant and droop characteristics using experimental results. In this way, appropriate representation of MG inertia constant based on types of committed units plays an important role [23]. On the other hand, successful operation of penetrated grid requires fast analysis approaches and the design of analytical methods to assess dynamics of interest. This helps TSOs to decide on re-dispatching of generating units to mitigate undesired dynamics. The proposed analysis method in this paper deals with highly uncertain behavior of penetrated grids by developing of a framework to represent the associated grid dynamics based on well-studied conventional grid behavior. Generally, the main contributions of this paper are threefold:

- Experimental derivation of MG equivalent model in both islanded and grid-connected modes. Such experimental validation can pave a novel way for the dynamic analysis of penetrated grids.
- Mathematical representation of MG inertia constant and droop characteristics based on types of committed DGs.
- Proposition of a parametric simple yet efficient approach to analytically investigate the effect of MGs penetration level on frequency

Downloaded from https://iranpaper.ir
https://www.tarjomano.com/order
ترجمه تخصصی این مقاله

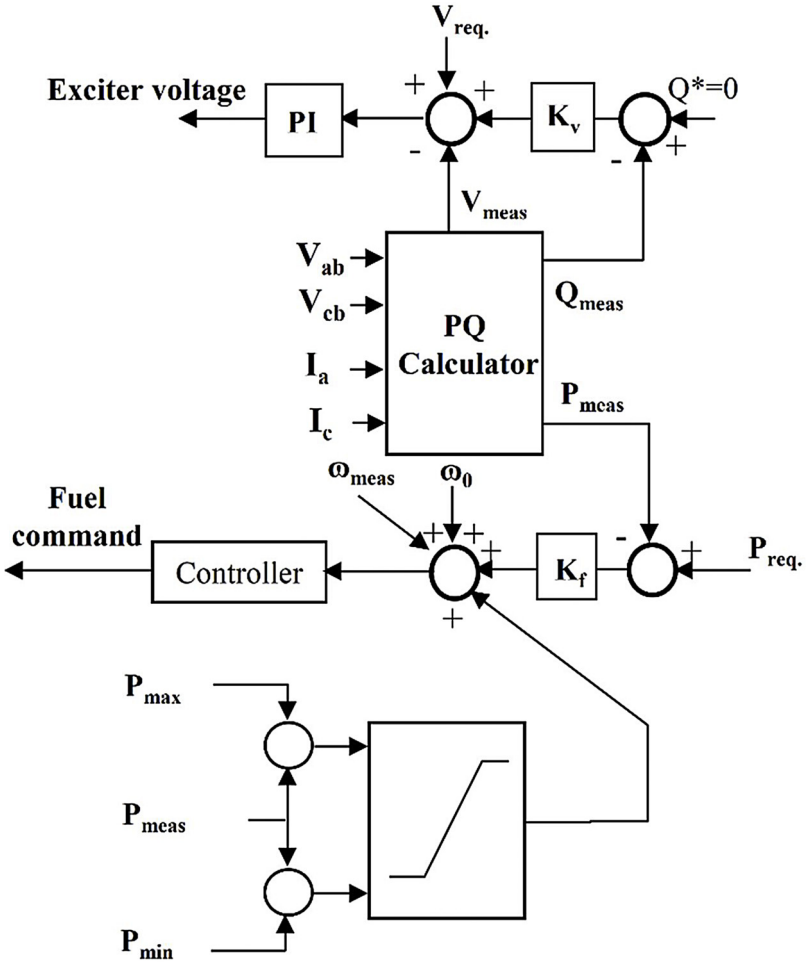

Fig. 2. Genset controller scheme.

dynamics. The method extends previous formulation of [6], developed by the author, to account for interconnected grid features and realistic dynamics of MGs. Simplicity and low computational time to deal with large system dynamics make the method suitable for real time applications.

2. Proposed analytical approach

2.1. Hypothesis

Several assumptions are introduced in the proposed framework to assess penetrated grid frequency dynamics. These are:

1 H and ω are the aggregated inertia constant and Center of Inertia (COI) speed, respectively.
2 Quasi steady state condition is employed for model derivation. This means that conventional assumption of constant frequency, i.e. nominal frequency for defining of all phasors and component reactances, is acceptable [4].
3 Voltage and rotor angle stabilities are assured using the developed control methodology by the author in Ref. [24].

2.2. Procedures

Developing of an approach to investigate the impacts of MGs penetration level on the host grid dynamics begins through defining of two systems, as follows:

a) Base system refers to as the original system without any MGs.
b) Penetrated system refers to as the base system in presence of MGs.

2.3. Analysis tools

In this research, three tools are used to deal with frequency stability assessment: *Matlab 2017b* including Power System Toolbox (PST) [25] in corporation with *PLECS* is used to perform dynamical simulation; *MAPLE 18* is also used for curve fitting purpose.

2.4. MG structure

The existing three-phase laboratory-scale MG in the Smart/Micro Grid Research Center (SMGRC) at University of Kurdistan (UOK) is employed for modeling purpose. The UOK-MG configuration, with 380 [V] nominal voltage and 50 [Hz] nominal frequency, as schematically represented in Fig. 1(a), is divided into two different parts: the AC part, where loads, diesel generators (Genset) and ESS are connected and the DC part where ESS, solar photovoltaic (PV) systems, and wind turbines are placed. While connection of the sources to the DC bus is carried out through DC/DC converters, the DC bus may be connected to main grid using DC/AC converters. Distributed energy resources within the MG include a 2×1 kW wind turbines, a 2 kW PV system, two diesel generators, including 1×5 kW and 1×10 kW, and 2×7 kW ESSs; the MG system includes also various static and dynamic loads (Fig. 1(b)). Inverters include Micro Replus and Power Inverters (SUN-10000) with power capacities ranging from 2 kW to 6 kW.

Downloaded from https://iranpaper.ir
https://www.tarjomano.com/order
ترجمه تخصصی این مقاله

2.5. MG modelling

This section begins with a sub-section devoted to modelling of DGs in grid-forming mode (islanded mode), and will be continued by deriving an experimental-based equivalent model of MG in grid-supporting mode (grid-connected mode). Experimental results of the UOK-MG in both modes may be compared with those of simulation results. A digital power system simulator is employed to realize host grid in grid-connected mode studies. This in turn allows to emulate important host grid parameters, such as inertia constant, to make the results realistic. Accordingly, results of UOK-MG in grid connected mode may be then extended to Multi-MGs to visualize high penetrated grid in Section 3.

a) Grid-forming mode

Genset includes an internal combustion engine driven by explosive combustion of gasoline and a field wound synchronous generator [26–28]. While a fuel command signal adjusts frequency of the Genset, terminal voltage may be controlled by exciter command signal [29–32]. Details of the controller are shown in Fig. 2.

It can be observed that the Genset behaves as a voltage source in the islanded mode and hence, power limiter is incorporated to impose limits on the output power. Some details of the model implementation are reported in Ref. [27]. Frequency dynamics of the Genset in response to switching on of a 4 kW Static Load Bank (SLB) at 2nd second of operation is shown in Fig. 3. Comparison of the experimental and simulation results reveals high efficiency of the model.

The same reasoning that is used to represent Genset behaviour in islanded mode can be extended to model inverter-based sources. However, the corresponding controller command signals are inverter frequency and voltage modulation index [33–35]. The modulation index is a scalar coefficient which in turn controls voltage at the inverter terminals [27]. Fig. 4 compares the ESS simulation results, obtained for switching on of 4 kW SLB at 1st second and switching off of 3 kW SLB at 5th seconds of the simulation, with those of experiments. Neglecting high frequency noise due to the switching of inverter's power transistors, the simulated waveforms for real and reactive powers follow the experimental results with high accuracy. The oscillation free behaviour of the simulated waveforms stems from the fact that the source of power is represented by an ideal voltage source with only fundamental frequency.

Of note that, the offset between the simulated and experimental reactive powers may be due to the neglecting of the line and transformer models.

- Supporting-grid mode

b.1) General equivalencing framework

In this subsection, an equivalent model of a grid-connected MG for frequency stability studies is proposed. General description of the proposed framework can be explained by the following steps:

Step 1: Set an initial assumption on number of operating points.

Step 2: Arbitrary Commitment of DGs in the UOK-MG to specify an operating point.

Step 3: Metering of the injected power of the MG to the host grid, i.e. P_{MG}.

Step 4: Modal analysis (Prony analysis) of the metered signal of Step 3 to calculate inertia constant. Applying Prony analysis to P_{MG} gives:

$$\frac{f}{P_{MG}} \propto \frac{a_i}{s + c_i} \rightarrow \frac{f}{P_{MG}} \propto \frac{1}{\frac{1}{a_i}s + \frac{c_i}{a_i}} \tag{1.a}$$

where, a, c are constant parameters which may be defined by Prony

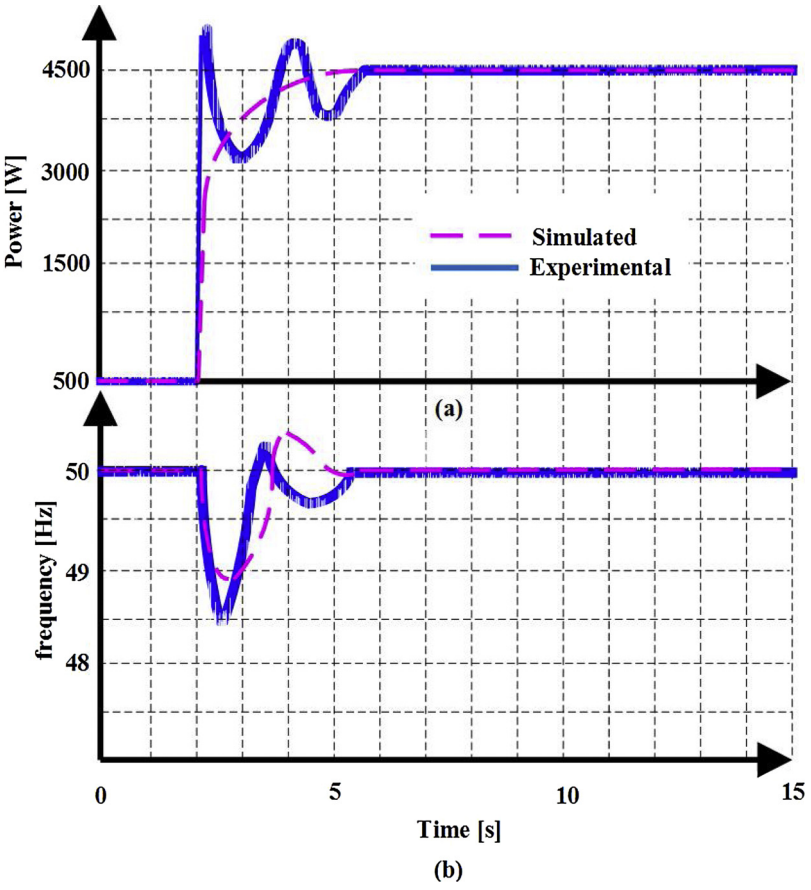

Fig. 3. Dynamics of Genset in response to switching on of 4 kW in 2nd second of the operation, (a) frequency response, (b) active power dynamics.

Downloaded from https://iranpaper.ir
https://www.tarjomano.com/order
ترجمه تخصصی این مقاله

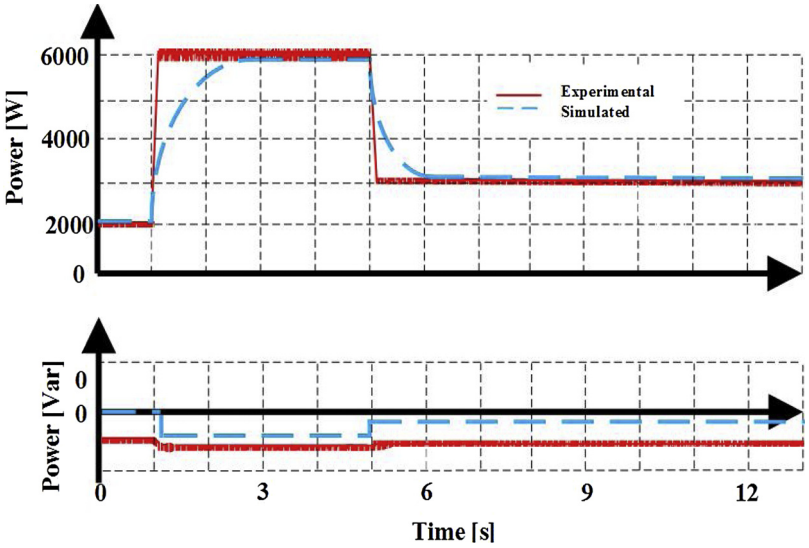

Fig. 4. Experimental and simulated waveforms for real and reactive power output for ESS operation in a UOK-MG.

analysis. Eq. (1.a) follows the same characteristics as classical swing equation of form:

$$\frac{f}{P_{MG}} \propto \frac{1}{M_i s + D_i} \tag{1.b}$$

where, M, and D define inertia constant and damping property, respectively. Hence, (1.a) with a reinterpretation of $\frac{1}{a_i} \triangleq M$; $\frac{c_i}{a_i} \triangleq D$ could be employed to calculate MG inertia constant.

Step 5: Return to Step 2, repeat until the pre-specified number of operating points are considered.

Step 6: Extract relationship, using curve fitting tools, between inertia constant and committed DGs.

The above steps are summarised in the flowchart of Fig. 5, and detailed discussions will be represented in what follows.

b.2) Detailed modelling procedure

In the previous work by the author [22], an approach for MG modeling has been introduced to represent associated behaviour with a simple equivalent model. Its use in the case of MG including ESS, considering capability to contribute in inertial response, is now reviewed to study transient frequency behavior. Indeed, a simple yet efficient equivalent model of MG is proposed, which in turn appropriately represents MGs special attributes in contributing in frequency control schemes. A schematic of the adopted model is shown in Fig. 6.

The figure reveals that MG dynamics, from upward point of view, would be mapped onto the conventional synchronous generator. Accordingly, the MG dynamics would be represented by the classical swing equation of form (1.a and 1.b). The quantity of interest to visualize (1.a and 1.b) is the injected power of the MG to the grid. A problem of interest, however, is that of calculating inertia of the equivalent MG in (1.a and 1.b).

To illustrate the proposed approach efficiency, the experimental results of the UOK-MG in grid-connected mode are utilized. Fig. 7 shows the dynamic performance of the MG, host grid and constituent DGs for a sequence of events.

While event # 1 refers to importing of power from the grid to the MG in response to re-dispatching of DGs, event # 2 refers to the islanding of MG from the grid. It can be observed that, between events # 1 and # 2, the host grid provides the required power of the MG with some inertia constant. Modal analysis of the injected power of the host grid to the MG in the transient period in Fig. 7, results in

$$\frac{\omega_{MG}}{\Delta P_{MG}} \cong \frac{0.37}{0.27 + 0.63s} \tag{2.a}$$

and for the steady state period, (2.a) would be re-written as:

$$\frac{\omega_{MG}}{\Delta P_{MG}} = 1000 \tag{2.b}$$

where, ω_{MGs} and ΔP_{MGs} are the frequency at the point of common coupling and the injected power of the MG, respectively.

Eq. (2.a) follows the same characteristics as (1.a and 1.b) and hence could be interpreted as a rotating mass. On the other hand, after settling of transients, (2.b) would represent MG behaviour. This bring a first order circuit response to a pulse function into mind. Therefore, the same reasoning that is used to assess a first order circuit in response to a pulse function could be adopted to approximate the effects of MG. In this way, one could represent the classical swing equation of MG as:

$$M_{MG}\frac{df(t)}{dt} = [T_m(t) - T_e(t)][u(\zeta) - u(\upsilon)] \tag{3}$$

where, ζ and υ $(\zeta < \upsilon)$ are DGs re-dispatching and islanding times, respectively.

Also, of interest, event # 2 refers to the islanding of MG where droop characteristic affects frequency response. The ratio of the grid power variation to the steady state frequency error of the islanded MG would be defined as droop characteristic. One could write this for Fig. 7 as:

$$R = \frac{\Delta P}{\Delta f} = \frac{\frac{0-1000}{5000}}{49.83 - 50} = 1.17\,[\frac{pu}{\text{Hz}}] \tag{4}$$

Finally, a relationship between inertia constant of (2.a) and MG capacity should be derived to facilitate assessment of impact of penetration level on the grid frequency dynamics. For this purpose, MG inertia constants, obtained by (2.a) for several operating points, may be plotted against the ratio of the Genset to the MG capacity, i.e. S_n, in Fig. 8.

In the figure, S_n, which defines by

$$S_n = \frac{P_{Genset}}{P_{MG}} = \frac{P_{Genset}}{P_{Genset} + P_{ESS} + P_{PV} + P_{WT}}$$

may be changed by re-commitment of the constituent Gensets. For this purpose, two Gensets with rated capacities of 5 kW and 10 kW with respectively 0.15 s and 0.21 s inertia constants are employed. This in turn produces three sets of data in Fig. 8. Moreover, to further generate data sets for model derivation, an analogue simulator, with inertia constant of 0.1 s, is utilized. The figure reveals that there is a direct relationship of form

Downloaded from https://iranpaper.ir
https://www.tarjomano.com/order
ترجمه تخصصی این مقاله

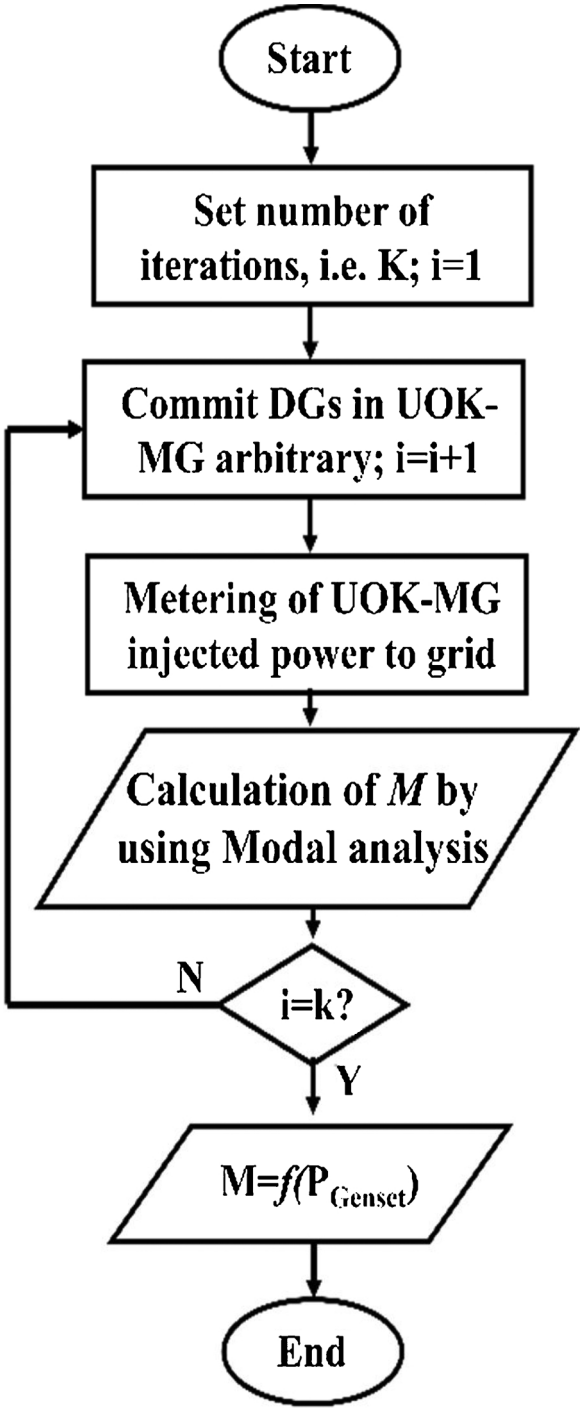

Fig. 5. Flowchart representation of the equivalencing approach.

$$H_{MG} = 1.6109S_n - 0.0644 \tag{5}$$

with Root Square (R^2) equal to 0.954.

2.6. Frequency dynamics criteria

Frequency response, as a measure of an interconnection's ability to stabilize frequency following a disturbance, would be assessed in respect to some indices, including Rate of Change of Frequency (*RoCoF*), frequency nadir and frequency evolution during time interval of interest [36]. These indices may be employed by TSOs and online monitoring and control systems to trigger protection devices, initiate load shedding and schedule/commit reserve power, respectively. Thus, accurate and timely estimation of these dynamics helps the associated entities to employ appropriate ancillary control schemes to ensure secure operation of the system. General description of the proposed approach to analytically estimate dynamics of interest can be explained by the following steps:

Step 1: Time Domain Simulation of a base system with specific parameters.

Step 2: Extracting of frequency dynamics of interest, including RoCoF, nadir and frequency evolution, from TDS result.

Step 3: Calculation of sensitivity factors of penetrated grid dynamics to the base system dynamics.

Step 4: Representing of penetrated grid dynamics based on the base system behaviour using sensitivity factors of Step 3.

The above steps are summarised in the flowchart of Fig. 9, and detailed discussions will be represented in what follows.

a) Rate of change of frequency (*RoCoF*)

ROCOF is the time derivative of the frequency (*df/dt*). The initial *RoCoF*, in response to a torque imbalance, is determined by the amount of stored rotational kinetic energy on the system [37]. Classical swing equation reveals that *RoCoF* is inversely proportional to the inertia constant, i.e. stored kinetic energy on the system. As there is a *RoCoF* standard of 0.5–1 Hz/s, penetrated system frequency assessment in compliance with *RoCoF* is of high importance.

Any disturbance in the system causes instantaneous frequency change in overall system Center of Inertia (COI), represented by [38,39]:

$$\frac{2M_{COI}}{\omega_0}\frac{d^2\theta}{dt^2} = \omega_{COI}(T_{mech} - T_{elec}) \xrightarrow{\theta=\omega_{COI}t-\omega_0 t+\theta_0} 2M_{COI}\frac{d(\Delta f_{COI})}{dt}$$
$$= 2\pi f_{COI}(T_{mech} - T_{elec}) \rightarrow$$
$$2M_{COI}(RoCoF_{COI}) = 2\pi f_{COI}(T_{mech} - T_{elec}) \tag{6}$$

where,

$$\Delta f_{COI} = \frac{\sum_i M_i \Delta f_i}{\sum M_i} \tag{7}$$

On the other hand, the interactions between areas as well as load dynamics (*D*) should be accounted for in the problem formulation to assess frequency dynamics in each area of an interconnected power system. In this way, (6) is rewritten for area *i* as [7]

$$\dot{f}_i = \frac{1}{2\pi M_i}[\Delta P_i - 2\pi D_i f_i - \sum_j P_{tie,ij}],\ i, j = 1,\ \ldots, n,\ i \neq j \tag{8}$$

where, $P_{tie,ij}$, and n are the transferred power between areas i and j and number of areas, respectively. Indeed, $P_{tie,ij}$ in (8) may be deviated from the pre-fault steady state value in response to the torque mismatch. Using Taylor expansion, one could write [6]:

$$P_{tie,0} + \Delta P_{tie} = P_{tie,0} + 2\pi P_{max}(f_i - f_j)\mathrm{Cos}(\delta_{i0} - \delta_{j0}).(\delta_i - \delta_j - \delta_{i0} - \delta_{j0}) +$$
$$[2\pi P_{max}(\dot{f}_i - \dot{f}_j)\mathrm{Cos}(\delta_{i0} - \delta_{j0}) - 2\pi P_{max}(f_i - f_j)\sin(\delta_{i0} - \delta_{j0})].$$
$$(\delta_i - \delta_j - \delta_{i0} - \delta_{j0})^2 \tag{9}$$

As there is no significant phase difference between frequencies at different areas of a strongly coupled network, $(\delta_i - \delta_j - \delta_{i0} - \delta_{j0})^2$ get a small value and thus the second term of right hand side of (9) could be neglected. Therefore, one could re-write (9) as

$$P_{tie,0} + \Delta P_{tie} = P_{tie,0} + 2\pi P_{max}(f_i - f_j)Cos(\delta_{i0} - \delta_{j0}).\Delta\delta \tag{10}$$

According to NERC standard, *RoCoF* defines as frequency deviation during 100 ms after occurrence of the fault. Accordingly, one could re-write (8) as:

Downloaded from https://iranpaper.ir
https://www.tarjomano.com/order
ترجمه تخصصی این مقاله

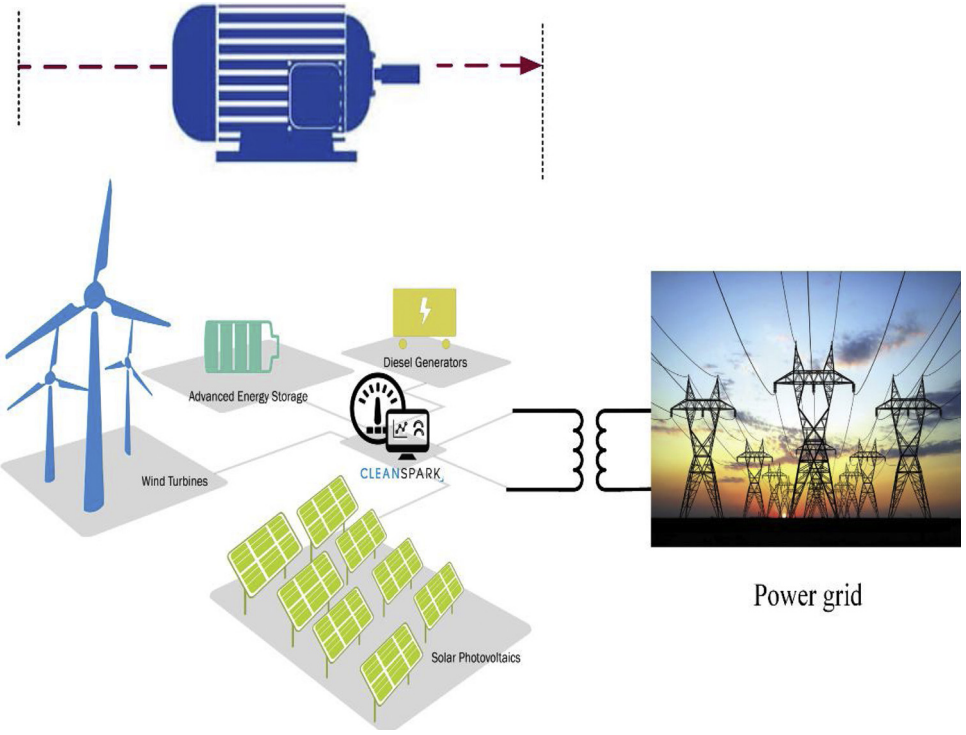

Fig. 6. Schematic of the proposed MG dynamic equivalent model.

$$\frac{f_i - 50}{0.1} = \frac{1}{2\pi M_i}[\Delta P_i - 2\pi D_i f_i - \sum_j P_{tie,ij}] \rightarrow f_i = 50 + \frac{0.1}{2\pi M_i}[\Delta P_i - 2\pi D_i f_i - \sum_j P_{tie,ij}] \quad (11)$$

Representation of *n-area* system dynamics by (6)–(11), gives *n-1* independent equations, with *n* unknown frequency, as represented by (12):

$$F_i(f_1, f_2, ..., f_j) + C_i = 0, j = 1, 2, ..., n, i = 1, 2, ..., n-1 \quad (12)$$

In order to deal with (12), the n^{th} equation would be formulated based on the *RoCoF* of the overall system COI, i.e. (6). This set calculates frequency, for 100 ms after the fault, in each area of the penetrated system. Therefore, *RoCoF* could be calculated by employing of $RoCoF = \frac{\Delta f}{0.1}$.

2.7. Frequency nadir

Frequency nadir defines as another index of interest to deal with penetrated system. According to the *Union for the Coordination of the Transmission of Electricity (UCTE)* standards [36], frequency nadir could be down up to 49.2 [Hz]. According to (6), the frequency response of the base system, for a given fault, may be written as:

$$2M_1 \frac{d(\Delta f_1)}{dt} = \omega_1(T_{mech} - T_{elec}) \quad (13.a)$$

and, one could re-write (13.a) as

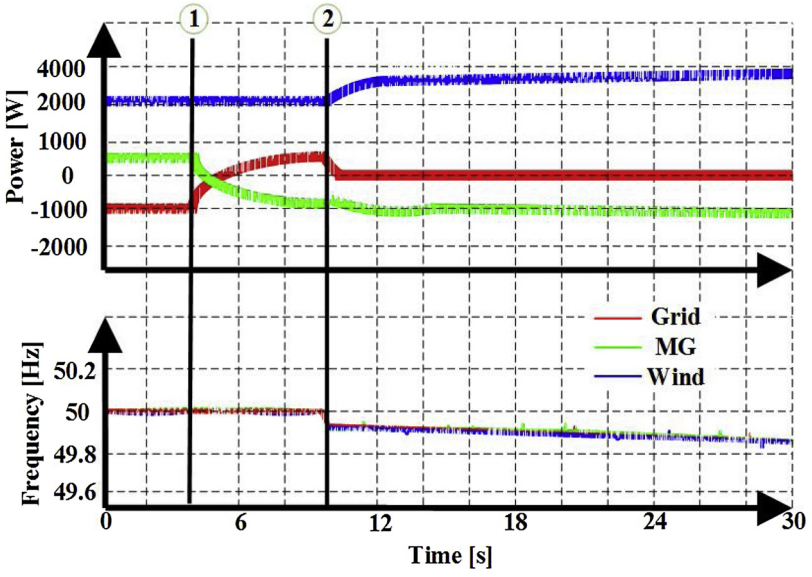

Fig. 7. Experimental waveforms for real power and frequency output for MG, wind turbine and host grid.

Downloaded from https://iranpaper.ir
https://www.tarjomano.com/order
ترجمه تخصصی این مقاله

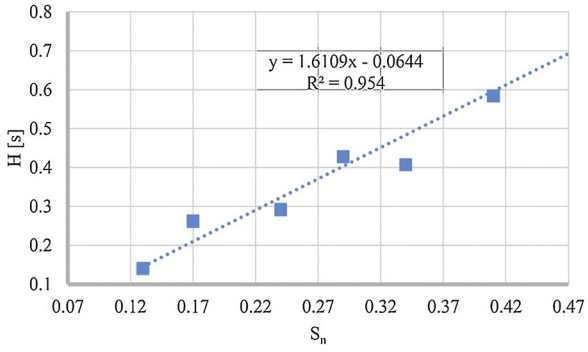

Fig. 8. Relationship between MG inertia and ratio of Genset to MG capacity.

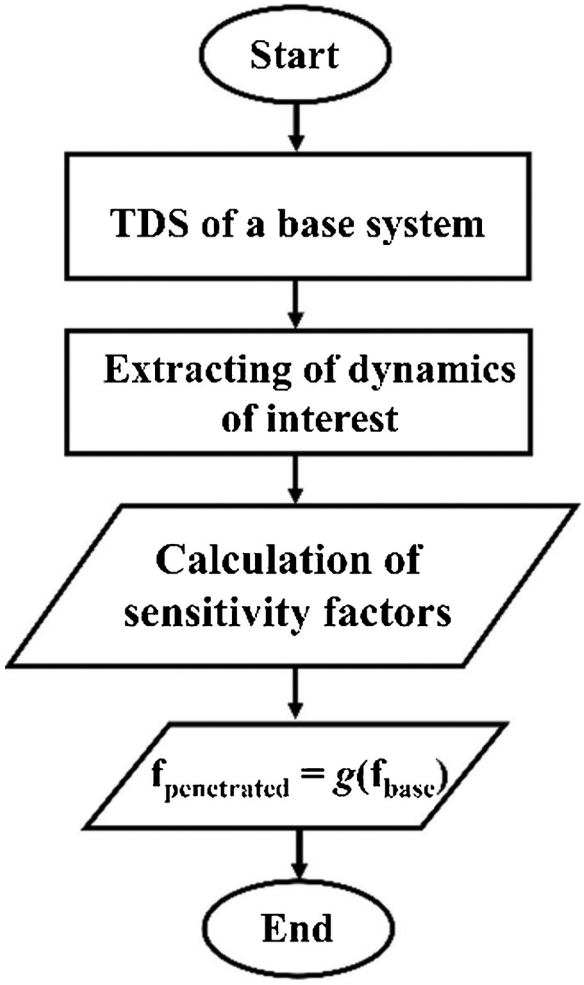

Fig. 9. Flowchart representation of the proposed analytical approach to estimate frequency dynamics.

$$2M_2\frac{d(\Delta f_2)}{dt} = \omega_2(T_{mech} - T_{elec}) \tag{13.b}$$

for the penetrated system. Dividing (13.b) by (13.a) gives:

$$\frac{M_2}{M_1}.\frac{RoCoF_2}{RoCoF_1} = \frac{2\pi f_2}{2\pi f_1} \rightarrow f_2 = \frac{M_2}{M_1}.\frac{RoCoF_2}{RoCoF_1}f_1 \tag{14}$$

Eq. (14) calculates the penetrated system nadir based on the *RoCoFs*, obtained using (12), and base system dynamics.

2.8. Delta frequency detection

The third dynamic of interest defines based on the introduced criterion by NERC Resource Subcommittee. It states that a frequency event is detected if during a time interval of interest, such as 15-s rolling time window, frequency deviation exceeds a specific threshold [40,41]. To proceed with this criterion, the frequency response of area *i* in Laplace domain of form [42]:

$$\Delta f_i(s) = -\frac{\Delta P_L - \frac{2\pi T_{ij}}{s}\Delta f_j(s)}{M_i s + \beta_i + \frac{2\pi T_{ij}}{s}} \tag{15}$$

is employed. In (15) β_i defines frequency bias of area *i*. By considering ΔP_{Li} in the form of a step function, one could re-write (15) as:

$$\Delta f_i(s) = -\frac{\Delta P_L - 2\pi T_{ij}\Delta f_j(s)}{M_i s^2 + \beta_i s + 2\pi T_{ij}} \tag{16}$$

In order to deal with the time domain criterion, inverse Laplace transformation of (16) is employed.

$$\Delta f_i(t) = -(\frac{\Delta P_L - 2\pi T_{ij}\Delta f_j}{M_i})(\frac{1}{p_1 - p_2})(e^{-p_2 t} - e^{-p_1 t}) \tag{17}$$

where, p_1, p_2 are the poles of (16). For a typical snapshot, at the end of the rolling window, frequency deviation is represented by

$$\Delta f_i(t + \Delta T) = -(\frac{\Delta P_L - 2\pi T_{ij}\Delta f_j}{M_i})(\frac{1}{p_1 - p_2})(e^{-a(t+\Delta T)} - e^{-b(t+\Delta T)}) \tag{18}$$

Dividing (18) by (17) and following the same procedure as (14) specify frequency deviation during time interval of interest for the penetrated system. In this way, all the variables have specific values except for term β_i. Steady state frequency deviation in both the base and reduced systems are employed to calculate β_i. For this purpose one could write

$$\beta_{2i} = \beta_{1i} \times \frac{\Delta f_{1i}^{steady-state}}{\Delta f_{2i}^{steady-state}} \tag{19}$$

Eq. (19) represents the penetrated system characteristics based on the base system features.

3. Simulation and results

The capability of the proposed method is investigated on the *New York/New England (NYNE) 68 Bus system* [25]. This system is a reduced order equivalent of the inter-connected New England Test System (NETS) and New York Power System (NYPS), with five geographical regions. NETS and NYPS are represented by a group of generators whereas, the power import from each of the three other neighboring areas are considered through equivalent generator models [43]. Single line diagram of this system is shown in Fig. 10. Twelve of the generators have power system stabilizers, tuned to provide sufficient damping. The system provides two types of load, including constant impedance and induction motors. The test systems data are taken from Ref. [44].

Eight scenarios are considered to assess the proposed formulations; they are derived from the shedding of loads and/or the tripping, without fault, of generating units. For instance, efficiency of the proposed method is illustrated by solving (12) for tripping generator number 13, a large and heavy loaded generating unit located in area 2. For the base system, frequency starts to decline from the nominal value and reaches 49.77 [Hz]. Area 2 Center-of-Inertia (COI) frequency responses of the base system (dashed line) and the penetrated system, obtained by TDS, for various penetration levels of 5.6%, 8% are shown in Fig. 11. The penetrated system would be realized by distributing the MG equivalent model, i.e. Eq. (3), in each PV bus according to the ratio of the associated bus generation to the area total generation capacity. Of note that, as NENY system is a strongly coupled network, there is no

Downloaded from https://iranpaper.ir
https://www.tarjomano.com/order
ترجمه تخصصی این مقاله

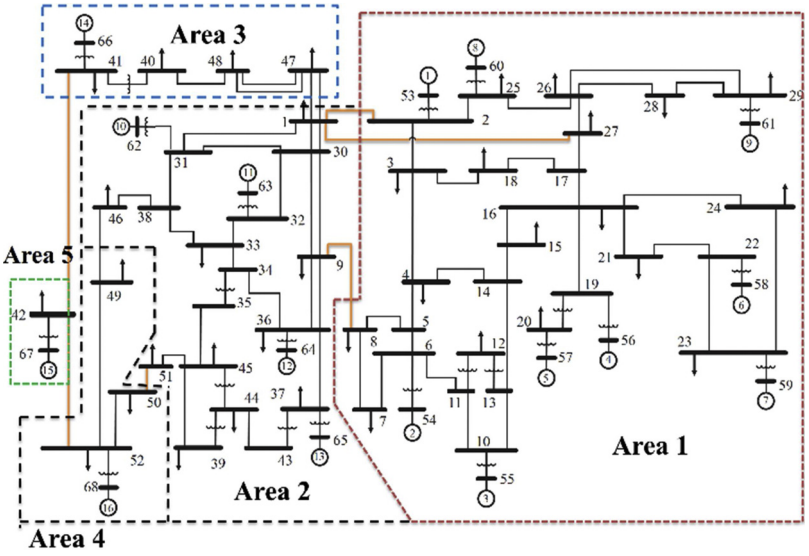

Fig. 10. Single line diagram of the 68-bus system showing coherent areas and their interconnections.

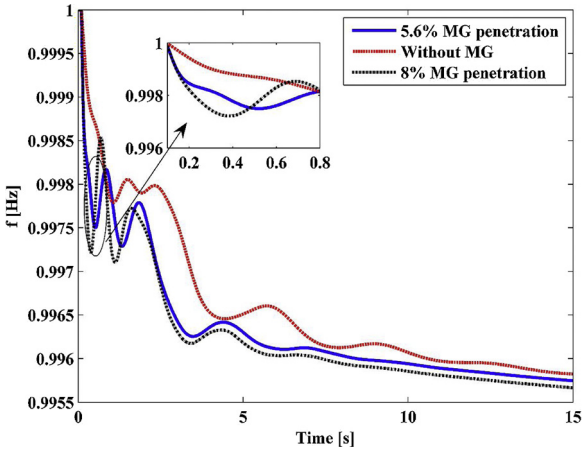

Fig. 11. Area 2 frequency in response to reduction of COI.

phase difference between frequencies at different zones and hence other areas also follow the same trace as Fig. 10. Moreover, center of gravity concept, proposed by the author in Ref. [4], could be employed to estimate local frequencies.

According to (12) and for the penetration level of 5.6%, one could write:

$$0.11f_1 + 0.33f_2 - 0.02f_3 - 0.15f_4 + 0.32f_5 = 0.092 \quad (20)$$

$$0.01f_1 + 0.43f_2 - 0.17f_3 - 0.27f_4 + 0.71f_5 = 0.312 \quad (21)$$

$$0.67f_1 + 0.03f_2 + 0.07f_3 - 0.83f_4 + 0.21f_5 = 0.762 \quad (22)$$

$$0.85f_1 + 0.12f_2 + 0.37f_3 - 0.29f_4 + 0.54f_5 = 0.341 \quad (23)$$

To complete the set of (20)–(23), Eq. (6) may be initialized as:

$$2M_{COI}\frac{d\left(\frac{\sum_i M_i\Delta f_i}{\sum M_i}\right)}{dt} = 2\pi f_{COI}(T_{mech} - T_{elec}) \rightarrow 2M_{COI}\sum_i \frac{M_i\dot{f}_i}{\sum_i M_i}$$
$$= 2\pi f_{COI}(T_{mech} - T_{elec}) \rightarrow$$
$$2M_{COI}\sum_i \frac{M_i f_i}{\sum_i M_i} = 0.2\pi f_{COI}(T_{mech} - T_{elec}) \rightarrow 0.32f_1 + 0.42f_2 + 0.54f_3$$
$$+ 0.76f_4 + 0.52f_5 = 0.12 \quad (24)$$

Table 1
Frequency dynamics error for 16-machine test system and 5.6% penetration level.

Scenario	Disturbance	Nadir error [%]	*RoCoF* error [%]	15-s error [%]
1	G_{12}	˜0	1.99	˜0
2	G_{13}	0.3	0.19	0.11
3	L_{14}	0.32	1.22	0.23
4	L_{15}	0.68	0.46	0.18
5	G_{16}	1.00	0.15	0.10
6	L_{37}	˜0	˜0	0.17
7	L_{42}	1.34	1.04	0.27
8	L_{52}	1.18	0.46	0.12

Also of interest, comparison between TDS results and the results of the proposed analytical method for penetration level of 8% are reported in Table 2.

Solving Eqs. (20)–(24) for period of 100 ms after fault occurrence leads to *RoCoF* of −0.73 [Hz/s] in area #2. This in turn causes 0.15% error in comparison with those of TDS of Fig. 11. Table 1 reports error of frequency nadir, *RoCoF* and frequency deviation in 15-s rolling window between the proposed method and TDS results. The results reported in Table 1 are associated with area 2 COI and stands for the penetration level of 5.6%.

Tables 1 and 2 results reveal that the proposed mathematical-based approach could accurately predict the impact of MG penetration level on the host grid frequency dynamics.

4. Conclusion

Fast response, wide-band performance and reconfigurable control of power electronic devices have caused many countries to set an ambitious target for power-electronics-enabled power systems. This in turn

Table 2
Frequency dynamics error for 16-machine test system and 8% penetration level.

Scenario	Disturbance	Nadir error [%]	*RoCoF* error [%]	15-s error [%]
1	G_{12}	˜0	0.81	˜0
2	G_{13}	0.13	˜0	˜0
3	L_{14}	˜0	0.38	˜0
4	L_{15}	0.68	0.69	0.41
5	G_{16}	˜0	˜0	0.03
6	L_{37}	˜0	0.09	0.07
7	L_{42}	0.74	0.21	0.07
8	L_{52}	1.98	0.12	0.72

Downloaded from https://iranpaper.ir
https://www.tarjomano.com/order
ترجمه تخصصی این مقاله

transforms system dynamics and brings new stability concerns as well as additional control flexibility. To deal with the emerging concerns, the UOK-MG experimental results are employed to derive MG equivalent model. Comparison of the experimental results with those of equivalent model demonstrates high accuracy of the proposed model. Afterwards, a mathematical-based approach is proposed to deal with frequency response of penetrated system. Indeed, an analytical approach is proposed in which could provide an efficient framework for TSOs to decide, based on the real time calculation of dynamics of interest, on re-dispatching of generating units through a centralized communication system. The results reveal that the proposed method could calculate the penetrated system frequency dynamics with error less than 2%.

Acknowledgment

This work was funded in part by the Iran National Science Foundation: INSF under Project 95824306 and in part by the Iran Grid Management Company (IGMC) under project 97/1927.

References

[1] N. Hatziargyriou, H. Asano, R. Iravani, C. Marnay, Microgrids: an overview of ongoing research, development, and demonstration projects, IEEE Power Energy Mag. (2007) 78–94.
[2] R.H. Lasseter, P. Piagi, Microgrid: a conceptual solution, IEEE Power Electronics Specialists Conference 6 (2004) 4285–4291.
[3] H. Bevrani, B. François, T. Ise, Microgrid Dynamics and Control, John Wiley & Sons, 2017.
[4] H. Golpîra, A.R. Messina, A center-of-gravity-based approach to estimate slow power and frequency variations, IEEE Trans. Power Syst. 33 (1) (2018) 1026–1035.
[5] F. Milano, F. Dörfler, G. Hug, D.J. Hill, G. Verbič, Foundations and challenges of low-inertia systems, 2018 Power Systems Computation Conference (PSCC), IEEE, 2018, pp. 1–25.
[6] H. Golpîra, H. Seifi, A.R. Messina, M.R. Haghifam, Maximum penetration level of micro-grids in large-scale power systems: frequency stability viewpoint, IEEE Trans. Power Syst. 31 (6) (2016) 5163–5171.
[7] A. Ulbig, T.S. Borsche, G. Andersson, Impact of low rotational inertia on power system stability and operation, IFAC Proc. Vol. 47 (3) (2014) 7290–7297.
[8] E. Vittal, A. Keane, M. O'Malley, Varying penetration ratios of wind turbine technologies for voltage and frequency stability, 2008 IEEE Power and Energy Society General Meeting-Conversion and Delivery of Electrical Energy in the 21st Century (2008) 1–6.
[9] G. Lalor, A. Mullane, M. O'Malley, Frequency control and wind turbine technologies, IEEE Trans. Power Syst. 20 (4) (2005) 1905–1913.
[10] K.A. Folly, S.P.N. Sheetekela, Impact of fixed and variable speed wind generators on the transient stability of a power system network, 2009 IEEE/PES Power Systems Conference and Exposition (2009) 1–7.
[11] A. Mitra, D. Chatterjee, A sensitivity based approach to assess the impacts of integration of variable speed wind farms on the transient stability of power systems, Renew. Energy 60 (2013) 662–671.
[12] F. Fernandez-Bernal, I. Egido, E. Lobato, Maximum wind power generation in a power system imposed by system inertia and primary reserve requirements, Wind Energy 18 (8) (2014) 1501–1514.
[13] R. Doherty, A. Mullane, G. Nolan, D.J. Burke, A. Bryson, M. O'Malley, An assessment of the impact of wind generation on system frequency control, IEEE Trans. Power Syst. 25 (1) (2010) 452–460.
[14] R. Yan, T.K. Saha, N. Modi, N.-A. Masood, M. Mosadeghy, The combined effects of high penetration of wind and PV on power system frequency response, Appl. Energy 145 (2015) 320–330.
[15] A.S. Ahmadyar, S. Riaz, G. Verbič, A. Chapman, D.J. Hill, A framework for assessing renewable integration limits with respect to frequency performance, IEEE Trans. Power Syst. 33 (4) (2018) 4444–4453.
[16] A. Keyhani, A. Chatterjee, Automatic generation control structure for smart power grids, IEEE Trans. Smart Grid 3 (3) (2012) 1310–1316.
[17] X. Chen, J. Lin, C. Wan, Y. Song, H. Luo, A unified frequency-domain model for automatic generation control assessment under wind power uncertainty, IEEE Trans. Smart Grid 10 (3) (2019) 2936–2947.
[18] B. Zaker, G.B. Gharehpetian, M. Karrari, Equivalent model parameter estimation of grid-connected fuel cell-based microgrid, Int. Trans. Electr. Energy Syst. (2018) e2540.
[19] W. Dai, J. Yu, X. Liu, W. Li, Two-tier static equivalent method of active distribution networks considering sensitivity, power loss and static load characteristics, Int. J. Electr. Power Energy Syst. 100 (2018) 193–200.
[20] M.M. Haji, W. Xu, G. Geng, Single-port and multi-port frequency-dependent network equivalents with numerically stable branches, IET Gener. Transm. Distrib. 12 (3) (2017) 564–570.
[21] S.M. Zali, J.V. Milanović, Generic model of active distribution network for large power system stability studies, IEEE Trans. Power Syst. 28 (3) (2013) 3126–3133.
[22] H. Golpîra, M.R. Haghifam, H. Seifi, Dynamic equivalencing of an active distribution network for large-scale power system frequency stability studies, IET Gener. Transm. Distrib. 9 (15) (2015) 2245–2254.
[23] N. Hatziargyriou, et al., Contribution to bulk system control and stability by distributed energy resources connected at distribution network, IEEE Power Energy Soc. (2017) Piscataway, NJ, USA, Rep. PES-TR22.
[24] H. Golpira, H. Bevrani, A.H. Naghshbandy, An approach for coordinated automatic voltage regulator—power system stabiliser design in large-scale interconnected power systems considering wind power penetration, IET Gener. Transm. Distrib. 6 (1) (2012) 39–49.
[25] J. Chow, G. Rogers, Power System Toolbox, Cherry Tree Scientific Software, [Online], Available: (2000) http://www.ecse.rpi.edu/pst/PST.html.
[26] H. Golpîra, M.R. Haghifam, H. Seifi, Dynamic power system equivalence considering distributed energy resources using Prony analysis, Int. Trans. Electr. Energy Syst. 25 (8) (2015) 1539–1551.
[27] M. Lemmon, Comparison of hardware tests with SIMULINK models of UW microgrid, Technical Report, Univ. Notre Dame, 2010 Available: https://www3.nd.edu/~lemmon/projects/Odyssian-2009/Vault/phase-2-monthly-reports/UW-Microgrid-Dynamics-modelsData.pdf.
[28] H. Nikkhajoei, R.H. Lasseter, Distributed generation interface to the CERTS microgrid, IEEE Trans. Power Deliv. 24 (3) (2009) 1598–1608.
[29] S. Krishnamurthy, T. Jahns, R. Lasseter, The operation of diesel gensets in a CERTS microgrid, Power and Energy Society General Meeting-Conversion and Delivery of Electrical Energy in the 21st Century, 2008 IEEE, IEEE, 2008, pp. 1–8.
[30] A. Renjit, M. Illindala, R. Lasseter, M. Erickson, D. Klapp, Modeling and control of a natural gas generator set in the CERTS microgrid, Energy Conversion Congress and Exposition (ECCE), 2013 IEEE, IEEE, 2013, pp. 1640–1646.
[31] M. Lemmon, Advanced Distribution and Control for Hybrid Intelligent Power Systems, Interim Technical Report, University of Notre Dame, 2011.
[32] S. Krishnamurthy, R. Lasseter, Control of wound field synchronous machine gensets for operation in a CERTS microgrid, Consort. Electr. Reliab. Technol. Solut. (2009).
[33] Y. Gao, Q. Ai, A distributed coordinated economic droop control scheme for islanded AC microgrid considering communication system, Electr. Power Syst. Res. 160 (2018) 109–118.
[34] M. Karami, H. Seifi, M. Mohammadian, Seamless control scheme for distributed energy resources in microgrids, IET Gener. Transm. Distrib. 10 (11) (2016) 2756–2763.
[35] G. Venkataramanan, M. Illindala, C. Houle, R. Lasseter, Hardware Development of a Laboratory-Scale Microgrid Phase 1: Single Inverter in Island Mode Operation, NREL Report No. SR-560-32527 Golden, CO: National Renewable Energy Laboratory, 2002.
[36] C.E.O.H. ENTSO-E, P1-Policy 1: Load-Frequency Control and Performance, (2009).
[37] H. Karimi, M. Karimi-Ghartemani, M.R. Iravani, Estimation of frequency and its rate of change for applications in power systems, IEEE Trans. Power Deliv. 19 (2) (2004) 472–480.
[38] H. Bevrani, Robust Power System Frequency Control, Springer, 2008.
[39] H. Golpira, A.R. Messina, H. Bevrani, Emulation of Virtual Inertia to Accommodate Higher Penetration Levels of Distributed Generation in Power Grids, IEEE Trans. Power Syst. (2019), https://doi.org/10.1109/TPWRS.2019.2908935.
[40] H.F. Illian, Frequency Control Performance Measurement and Requirements, Lawrence Berkeley National Laboratory, 2011.
[41] Nerc, Standard BAL-003-1—Frequency Response and Frequency Bias Setting, (2013) https://www.nerc.com/pa/Stand/Project%20200712%20Frequency%20Response%20DL/Mapping_Table_BAL-003-0_to_BAL-003-1-090611.pdf.
[42] H. Bevrani, T. Hiyama, Intelligent Automatic Generation Control, CRC Press, 2017.
[43] D.H. Wilson, K. Hay, G.J. Rogers, Dynamic model verification using a continuous modal parameter estimator, 2003 IEEE Bologna Power Tech Conference Proceedings 2 (2003) 6.
[44] G. Rogers, Power System Oscillations, Springer Science & Business Media, 2012.